

REANALYSIS OF THE GRAVITATIONAL MICROLENSING EVENT MACHO-97-BLG-41 BASED ON COMBINED DATA

YOUN KIL JUNG¹, CHEONGHO HAN^{1,4}, ANDREW GOULD², AND DAN MAOZ³

¹Department of Physics, Institute for Astrophysics, Chungbuk National University, Cheongju 371-763, Korea

²Department of Astronomy, Ohio State University, 140 West 18th Avenue, Columbus, OH 43210, USA and

³School of Physics and Astronomy, Tel-Aviv University, Tel Aviv 69978, Israel

Draft version August 26, 2024

ABSTRACT

MACHO-97-BLG-41 is a gravitational microlensing event produced by a lens composed of multiple masses detected by the first-generation lensing experiment. For the event, there exist two different interpretations of the lens from independent analyses based on two different data sets: one interpreted the event as produced by a circumbinary planetary system while the other explained the light curve with only a binary system by introducing orbital motion of the lens. According to the former interpretation, the lens would be not only the first planet detected via microlensing but also the first circumbinary planet ever detected. To resolve the issue using state-of-the-art analysis methods, we reanalyze the event based on the combined data used separately by the previous analyses. By considering various higher-order effects, we find that the orbiting binary-lens model provides a better fit than the circumbinary planet model with $\Delta\chi^2 \sim 166$. The result signifies the importance of even and dense coverage of lensing light curves in the interpretation of events.

Subject headings: gravitational lensing: micro – planetary systems – binaries: general

1. INTRODUCTION

The last two decades have witnessed tremendous progress in gravitational microlensing experiments. On the observational side, improvement in both hardware and software has contributed to the great increase of the detection rate of lensing events from tens of events per year at the early stage of the experiments to thousands per year at the current stage. In addition, photometry based on difference imaging substantially improved the quality of photometry.

Along with the observational progress, there also has been advance on the analysis side. A good example is the analysis of light curves of lensing events produced by multiple masses. The light curve of a single-lens event is described by a simple analytic equation with a small number of parameters and the lensing magnification varies smoothly with respect to the lensing parameters. As a result, observed light curves can be easily modeled by a simple χ^2 minimization method. However, when events are produced by multiple masses, modeling light curves becomes very complex not only because of the increased number of lensing parameters but also because of the non-linear variation of lensing magnification with respect to the parameters. The non-linearity of lensing magnifications is caused by the formation of caustics which denote positions on the source plane where the lensing magnification of a point source diverges. Caustics cause difficulties in lens modeling in two ways. First, they make it difficult to use a simple linearized χ^2 minimization method in modeling light curves because of the complexity of the parameter space caused by the singularity. Second, magnification computations for source positions on a caustic are numerically intensive. As a result, modeling a multiple lens event was a daunting task at the early stage of lensing experiments. However, with the introduction of efficient non-linear modeling methods such as the Markov Chain Monte Carlo (MCMC) algorithm, combined with advances in computer technology such as computer clusters or

graphic processing units, precise and fast modeling became possible and now it is routine to model light curves in real time as lensing events progress (Dong et al. 2006; Cassan 2008; Kains et al. 2009; Bennett 2010; Ryu et al. 2010; Bozza et al. 2012). Furthermore, current modeling take into account various subtle higher-order effects.

In this paper, we reanalyze the lensing event MACHO-97-BLG-41 that is a multiple-lens event detected by the first-generation lensing experiment Massive Compact Halo Objects (MACHO: Alcock et al. 1993). For the event, there exist two different interpretations. Based mainly on the data obtained from the MACHO experiment, Bennett et al. (1999) interpreted the event as produced by a circumbinary planetary system where a planet was orbiting a stellar binary. On the other hand, Albrow et al. (2000), from independent analysis based on a different data set obtained by the Probing Lensing Anomalies NETWORK (PLANET: Albrow et al. 1998) group, arrived at a different interpretation that the light curve could be explained without the introduction of a planet but rather by considering the orbital motion of the binary lens. According to the interpretation of Bennett et al. (1999), the lowest-mass component of the triple-mass lens would be not only the first planet detected via microlensing but also the first circumbinary planet ever detected. Despite the importance of the event, the issue of its correct interpretation remains unresolved. Therefore, we revisit MACHO-97-BLG-41, applying state-of-the-art analysis methods to the combined data used separately by Bennett et al. (1999) and Albrow et al. (2000).

2. DATA

The data used for our analysis come broadly from two streams. The first stream comes from MACHO survey observations plus the Global Microlensing Alert Network (GMAN: Alcock et al. 1997) and Microlensing Planet Search (MPS: Rhie et al. 1999) follow-up observations. We refer to this data set as the “MACHO data”. The other stream comes from observations conducted by the PLANET group. We denote this data set as the “PLANET data”. In Table 1, we present tele-

⁴ Corresponding author

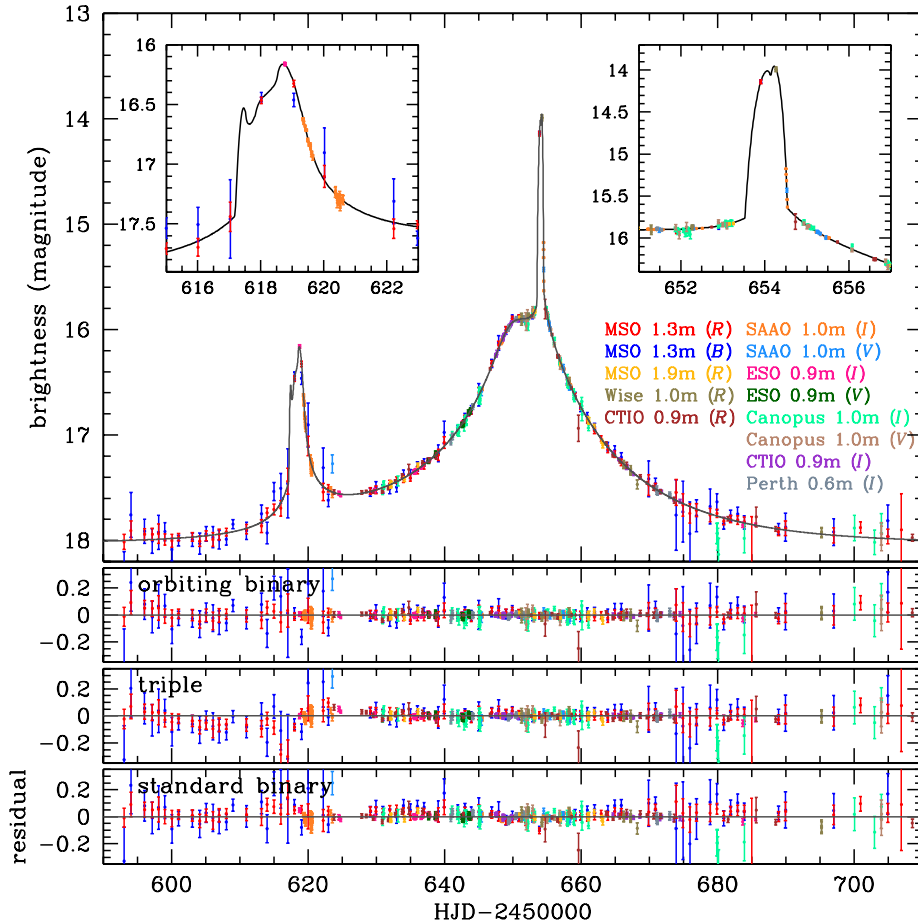


FIG. 1.— Light curve of MACHO-97-BLG-41 based on the combined MACHO plus PLANET data sets. Also presented is the best-fit model curve from our analysis. The two insets in the upper panel show the enlarged view of the two caustic-involved features at $\text{HJD}' \sim 619$ and 654. The lower three panels show the residual from the orbiting binary, triple, and static binary lens models.

TABLE 1
DATA SETS

MACHO data		PLANET data	
observatory	number	observatory	number
MSO 1.3 m (R)	711	SAAO 1.0 m (I)	97
MSO 1.3 m (B)	772	SAAO 1.0 m (V)	14
MSO 1.9 m (R)	16	ESO/Dutch 0.9 m (I)	58
Wise 1.0 m (R)	17	ESO/Dutch 0.9 m (V)	18
CTIO 0.9 m (R)	35	Canopus 1.0 m (I)	95
		Canopus 1.0 m (V)	14
		CTIO 0.9 m (I)	49
		Perth 0.6 m (I)	26

NOTE. — MSO: Mount Stromlo Observatory; CTIO: Cerro Tololo Inter-American Observatory, SAAO: South Africa Astronomy Astronomical Observatory, ESO: European Southern Observatory.

scopes, passbands, and the number of data of the individual data sets. Note that Bennett et al. (1999) analyzed only the MACHO data set while Albrow et al. (2000) conducted their analysis based only on the PLANET data set.

In order to use data sets obtained from different observatories, we rescale error bars. For this, we first readjust error bars so that the cumulative distribution of χ^2/dof ordered by magnifications matches to a standard cumulative distribution of Gaussian errors by introducing a quadratic error term (Bachelet et al. 2012). Then, error bars are rescaled so that χ^2/dof becomes unity, where χ^2 is derived from the best-fit

solution. During this normalization process, 3σ outliers from the solution are removed to minimize their effect on modeling.

In Figure 1, we present the light curve based on the combined MACHO + PLANET data. The light curve is characterized by two separate peaks at $\text{HJD}' = \text{HJD} - 2450000 \sim 619$ and 654. We note that the models of Bennett et al. (1999) and Albrow et al. (2000) are consistent in the interpretation of the overall light curve including the peak at $\text{HJD}' \sim 654$. However, the two models differ in the interpretation of the peak at $\text{HJD}' \sim 619$. While Bennett et al. (1999) explained the first peak by introducing an additional lens component of a circumbinary planet, Albrow et al. (2000) described the peak by considering the orbital motion of the binary lens.

3. ANALYSIS

3.1. Standard Binary-lens Model

To describe the observed light curve of the event, we begin with a standard binary-lens model. Basic description of a binary-lens event requires seven lensing parameters. The first three of these parameters describe the geometry of the lens-source approach including the time of the closest lens-source approach, t_0 , the lens-source separation (normalized by the angular Einstein radius of the lens, θ_E) at that moment, u_0 , and the time scale for the source to cross the Einstein radius, t_E (Einstein time scale). Another three parameters describe the binary nature of the lens including the projected separa-

TABLE 2
 BEST-FIT PARAMETERS

parameter	binary lens			triple lens	
	standard	orbit	orbit+parallax	standard	parallax
χ^2/dof	2355.8/1920	1915.1/1920	1912.4/1920	2086.6/1920	2077.3/1920
t_0 (HJD')	653.519 ± 0.004	653.426 ± 0.006	653.426 ± 0.007	653.371 ± 0.008	653.388 ± 0.008
u_0 (10^{-2})	8.123 ± 0.024	-7.346 ± 0.079	7.303 ± 0.074	7.407 ± 0.047	7.284 ± 0.049
t_E (days)	20.26 ± 0.016	24.11 ± 0.229	23.95 ± 0.213	24.82 ± 0.155	24.50 ± 0.150
s_1	0.494 ± 0.0003	0.479 ± 0.002	0.481 ± 0.002	0.485 ± 0.002	0.480 ± 0.002
q_1	0.481 ± 0.003	0.346 ± 0.005	0.342 ± 0.005	0.318 ± 0.005	0.326 ± 0.005
α	1.211 ± 0.003	-1.176 ± 0.003	1.179 ± 0.003	1.152 ± 0.003	1.156 ± 0.005
s_2				1.900 ± 0.007	1.875 ± 0.008
q_2 (10^{-3})				5.149 ± 0.160	4.644 ± 0.180
ψ				1.872 ± 0.003	1.858 ± 0.008
ρ_* (10^{-3})	9.69 ± 0.08	7.49 ± 0.12	7.91 ± 0.11	7.36 ± 0.09	7.35 ± 0.01
$\pi_{E,N}$			-1.59 ± 0.38		0.21 ± 0.15
$\pi_{E,E}$			0.29 ± 0.10		0.34 ± 0.08
ds/dt (yr^{-1})		-0.72 ± 0.050	-0.67 ± 0.05		
$d\alpha/dt$ (yr^{-1})		-0.95 ± 0.037	-0.30 ± 0.16		

tion s (in units of θ_E) and the mass ratio q between the binary-lens components, and the source trajectory angle with respect to the binary axis α . The two peaks of the light curve of MACHO-97-BLG-41 are likely to be features involved with caustic crossings or approaches during which finite-source effect becomes important (Dominik 1995; Gaudi & Gould 1999; Gaudi & Petters 2002). To account for this effect, an additional parameter, the normalized source radius $\rho_* = \theta_*/\theta_E$ is needed, where θ_* is the angular source radius. In our standard binary-lens modeling, we additionally consider the limb-darkening variation of the source star surface brightness by introducing linear-limb-darkening coefficients, Γ_λ . The surface brightness profile is modeled as $S_\lambda \propto 1 - \Gamma_\lambda(1 - 3\cos\phi/2)$, where λ denotes the observed passband and ϕ is the angle between the normal to the surface of the source and the line of sight toward the source (Albrow et al. 1999). Based on the source type (subgiant) determined by the spectroscopic observation conducted by Lennon et al. (1997), we adopt coefficients from Claret (2000). The adopted values are $\Gamma_B = 0.793$, $\Gamma_V = 0.666$, $\Gamma_R = 0.575$, and $\Gamma_I = 0.479$ for data sets acquired with a standard filter system. For the MSO 1.3m data, which used a non-standard filter system, we adopt $(\Gamma_B + \Gamma_V)/2$ for the B -band data and $(\Gamma_R + \Gamma_I)/2$ for the R -band data.

Although the two sets of solutions presented by Bennett et al. (1999) and Albrow et al. (2000) already exist, we separately search for solutions in the vast parameter space encompassing wide ranges of binary separations and mass ratios in order to check the possible existence of other solutions. From this, we find a unique solution with $s \sim 0.49$ and $q \sim 0.48$. See Table 1 for the complete solution of the model. We note that the solution is basically consistent with the results of Bennett et al. (1999) and Albrow et al. (2000) in the interpretation of the main part of the light curve including the peak at $\text{HJD}' \sim 654$. At the bottom panel of Figure 1, we present the residual of the standard binary model. It is found that there exist some significant residuals for the standard model. This is also consistent with the previous analyses that a basic binary model is not adequate to precisely describe the light curve.

3.2. Higher-order Effects

The existence of residuals in the fit of the standard binary lens model suggests the need for considering higher-order effects. We consider the following effects.

First, we consider the effect of the motion of an observer

caused by the orbital motion of the Earth around the Sun. This ‘‘parallax’’ effect causes the source trajectory to deviate from rectilinear, resulting in long-term deviations in lensing light curves (Gould 1992). The event MACHO 97-BLG-41 lasted ~ 100 days, which is an important portion of the Earth’s orbital period, i.e. 1 year, and thus the parallax effect can be important. Considering the parallax effect requires two additional parameters $\pi_{E,N}$ and $\pi_{E,E}$, that are the two components of the lens parallax vector π_E projected onto the sky along the north and east equatorial coordinates, respectively. The magnitude of the parallax vector corresponds to the relative lens-source parallax, $\pi_{\text{rel}} = AU(D_L^{-1} - D_S^{-1})$, scaled to the Einstein radius of the lens, i.e. $\pi_E = \pi_{\text{rel}}/\theta_E$ (Gould 2004).

Second, the orbital motion of a binary lens can also cause the source trajectory to deviate from rectilinear (Dominik 1998). The orbital motion causes further deviations in lensing light curves by deforming the caustic over the course of the event. The ‘‘lens orbital’’ effect can be important for long time-scale events produced by close binary-lens events for which the event duration comprises an important portion of the orbital period of the lens system (Shin et al. 2013). To first order approximation, the lens orbital motion is described by two parameters, ds/dt and $d\alpha/dt$, that represent the change rates of the normalized binary separation and the source trajectory angle, respectively (Albrow et al. 2000).

Third, we also check the possible existence of a third body in the lens system. Introducing an additional lens component requires three additional lensing parameters including the normalized projected separation, s_2 , and the mass ratio, q_2 , between the primary and the third body, and the position angle of the third body with respect to the line connecting the primary and secondary of the lens, ψ .

3.3. Result

We test models considering various combinations of the higher-order effects. In Table 2, we list the goodness of the fits and the best-fit parameters for the individual tested models. From the comparison of the models, we find the following results.

First, we confirm the result of Albrow et al. (2000) that the consideration of the orbital effect substantially improves the fit. We find that the improvement is $\Delta\chi^2 \sim 441$ compared to the static binary model. When we additionally consider the parallax effect, the improvement of the fit, $\Delta\chi^2 \sim 2.7$, is very

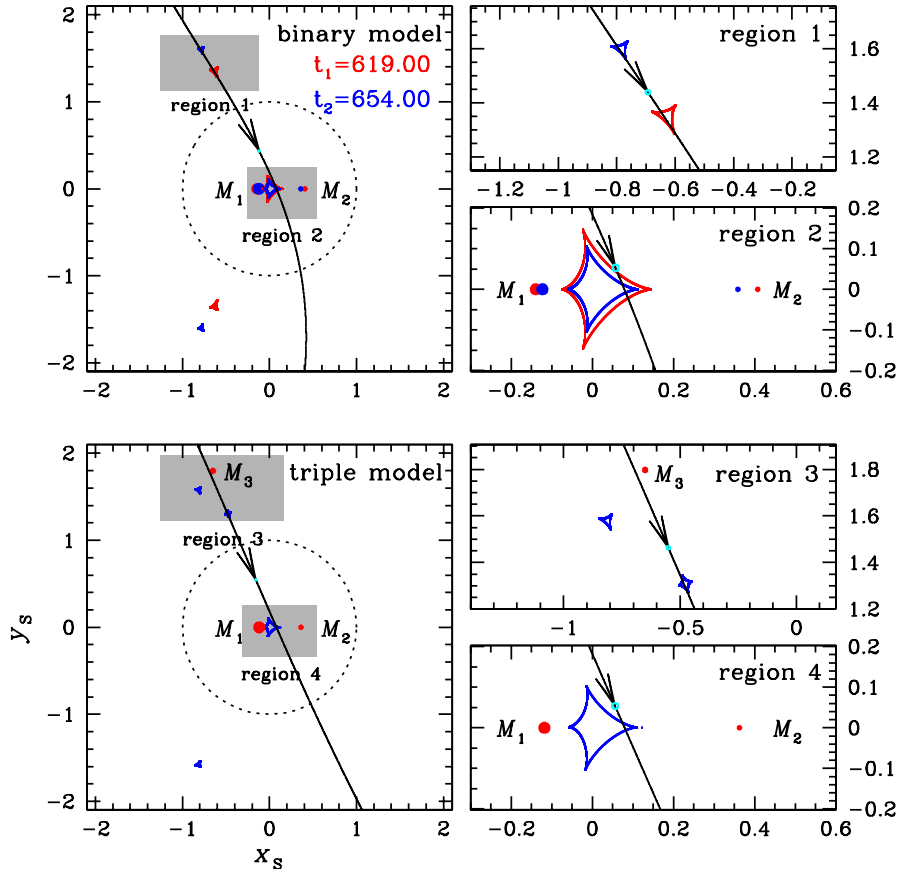


FIG. 2.— Geometry of the lens system for the best-fit binary (upper panels) and triple (lower panels) lens solutions. In each panel, the closed cuspy figures represent caustics and the curve with an arrow is the source trajectory. The filled circles is the locations of the lens components and the dotted circle is the Einstein ring centered at the barycenter of the lens. Right panels show the enlarged view of the corresponding shaded regions in the left panels. For the binary model, caustics and lens positions vary in time due to the orbital motion. We present two sets of caustics at HJD' = 619 and 654. The coordinates are co-rotating with the binary axis so that the binary axis aligns with the abscissa. All lengths are scaled by the Einstein radius θ_E .

meager. This implies that among the two effects, the orbital motion of the lens is the dominant higher-order effect in explaining the residual from the standard model. In Figure 1, we present the model light curve on the top of the observed light curve and the residual of the model. In Figure 2, we also present the geometry of the lens system.

Second, we find that the existence of a third body does not provide a fully acceptable fit. Our best-fit solution of three-body lens modeling is consistent with the solution of Bennett et al. (1999) in the sense that the third body is a circumbinary planet with a small mass ratio. See Table 2 for the best-fit parameters and Figure 2 for the lens system geometry. With the introduction of a planetary third body, the fit does improve from the standard binary model with $\Delta\chi^2 \sim 270$. The additional consideration of the parallax effect further improves the fit with $\Delta\chi^2 \sim 9$, but it is still substantially poorer than the orbiting binary-lens model with $\Delta\chi^2 \sim 166$. From the comparison of the residual (see Figure 1), it is found that the triple lens model cannot precisely describe the light curve during and before the first peak, $595 \lesssim \text{HJD}' \lesssim 625$.

The key PLANET data that exclude the triple lens are from SAAO. Their smooth “parabolic” decline signals a caustic exit along the axis of cusp. This is compatible with the triangular caustic generated by the close binary, but not with the quadrilateral caustic induced by the putative planet. In partic-

ular, the near-symmetric shape of the quadrilateral caustic implies that a cusp-axis trajectory would have a near-symmetric excess flux in the approach to the first peak as after its exit, which is not seen in the pre-peak MSO data.

4. CONCLUSION

We have conducted a reanalysis of the event MACHO-97-BLG-41 for which there exist two different interpretations. From the analysis considering various higher-order effects based on the combined data sets used separately by the previous analyses, we find that the dominant effect for the deviation from the standard binary-lens model is the orbital motion of the binary lens.

The result signifies the importance of even and dense coverage of lensing light curves for correct interpretation of gravitational lenses. For MACHO-97-BLG-41, the difference between the two previous interpretations partially stems from the poor coverage of the first peak that is important in the interpretation. Although a strategy based on survey plus follow-up observations can densely cover anomalies occurring at an expected time (e.g., peak of a high-magnification event) or long-lasting anomalies, it would be difficult to densely cover short-lasting anomalies arising abruptly at an unexpected moment. Since the first-generation lensing experiments, there has been great progress in survey experiments. The cadence of survey observations has increased from ~ 1 –

2 per day to several dozens a day for the current lensing experiments (OGLE: Udalski (2003), MOA: Bond et al. (2001), Sumi et al. (2003), Wise: Shvartzvald & Maoz (2012)). Furthermore, a new survey based on a network of multiple telescopes (KMTNet: Korea Microlensing Telescope Network) equipped with large format cameras is planned to achieve a cadence of more than 100 per day. With improved coverage,

the characterization of microlenses by future surveys will be more accurate.

Work by CH was supported by Creative Research Initiative Program (2009-0081561) of National Research Foundation of Korea. AG was supported by NSF grant AST 1103471. DM and AG acknowledge support by the US Israel Binational Science Foundation.

REFERENCES

- Albrow, M. D., Beaulieu, J. -P., Birch, P., et al. 1998, *ApJ*, 509, 687
 Albrow, M. D., Beaulieu, J. -P., Caldwell, J. A. R., et al. 1999, *ApJ*, 522, 1022
 Albrow, M. D., Beaulieu, J. -P., Caldwell, J. A. R., et al. 2000, *ApJ*, 534, 894
 Alcock, C., Akerlof, C. W., Allsman, R. A., et al. 1993, *Nature*, 365, 621
 Alcock, C., Allen, W. H., Allsman, R. A., et al. 1997, *ApJ*, 491, 436
 Bachelet, E., Shin, I. -G., Han, C., et al. 2012, *ApJ*, 754, 73
 Bennett, D. P. 2010, *ApJ*, 716, 1408
 Bennett, D. P., Rhie, S. H., Becker, A. C., et al. 1999, *Nature*, 402, 57
 Bond, I. A., Abe, F., Dodd, R. J., et al. 2001, *MNRAS*, 327, 868
 Bozza, V., Dominik, M., Rattenbury, N. J., et al. 2012, *MNRAS*, 424, 902
 Cassan, A. 2008, *A&A*, 491, 587
 Claret, A. 2000, *A&A*, 363, 1081
 Dominik, M. 1995, *A&AS*, 109, 597
 Dominik, M. 1998, *A&A*, 329, 361
 Dong, S., Depoy, D. L., Gaudi, B. S., et al. 2006, *ApJ*, 642, 842
 Gaudi, B. S., & Gould, A. 1999, *ApJ*, 513, 619
 Gaudi, B. S., & Petters, A. O. 2002, *ApJ*, 580, 468
 Gould, A. 1992, *ApJ*, 392, 442
 Gould, A. 2004, *ApJ*, 606, 319
 Kains, N., Cassan, A., Horne, K., et al. 2009, *MNRAS*, 395, 787
 Lennon, D. J., Mao, S., Reetz, J., et al. 1997, *ESO Messenger*, 90, 30
 Rhie, S. H., Becker, A. C., Bennett, D. P., et al. 1999, *ApJ*, 522, 1037
 Ryu, Y.-H., Han, C., Hwang, K.-H., et al. 2010, *ApJ*, 723, 81
 Shin, I. -G., Sumi, T., Udalski, A., et al. 2013, *ApJ*, 764, 64
 Shvartzvald, Y. & Maoz, D. 2012, *MNRAS*, 419, 3631
 Sumi, T., Abe, F., Bond, I. A., et al. 2003, *ApJ*, 591, 204
 Udalski, A. 2003, *Acta Astron.*, 53, 291